A new technique for quick identification of defective region inside γ-ray detector

Biswajit Das*, R. Palit, A. Kundu, P. Dey, V. Malik, S. K. Jadav, B. S. Naidu, and A. T. Vazhappilly

Department of Nuclear and Atomic Physics
Tata Institute of Fundamental Research, Mumbai - 400005, India

(*) biswajit.das@tifr.res.in

***Abstract*—The γ-ray detection efficiency of a detector decreases over time due to factors like radiation damage or an increase in the thickness of the inactive dead layer. For large γ-ray detector facilities, it is crucial to assess the health condition and performance of the inner regions of the detector crystals over time. In this study, we have introduced a method using GEANT4 simulation to detect defective regions within thick γ-ray detectors. In the experimental phase, a scanning setup was employed, comprising a single-crystal High Purity Germanium (HPGe) detector and a position-sensitive GAGG:Ce detector for coincidence measurements, using a ^{22}Na source. The 2D images were reconstructed from the front-face and side-face scans of the single-crystal coaxial HPGe detector, employing an energy gate set at 511 keV. A position gate applied to a specific section of those 2D images allowed for the mapping of γ-ray interactions along a conical path within the HPGe detector. The methodology involved the comparison and analysis of histograms generated from various sector gates, facilitating the identification of the defective region's position. In the GEANT4 simulation, a defective region was defined within the crystal, and that was effectively represented in the corresponding scanned image, which exhibited reduced efficiency. It's important to note that this method's effectiveness is restricted by the absorption profile of the 511 keV γ-ray, limiting its applicability to a depth of approximately 4 cm from the surface of the HPGe crystal. However, this approach can offer a swift and convenient method for inspecting γ-ray detectors, making it a valuable tool for the detector industry.**

***Keywords* — defective/damaged region identification of HPGe crystal; γ-ray tracking; position-sensitive GAGG; GEANT4 simulation**

I. Introduction

Since the discovery of nuclear decay, γ-ray detection has been extensively utilized for various nuclear structure investigations. Additionally, it also plays a crucial role in the field of nuclear medicine [1–4]. In contemporary times, the utilization of γ-ray detectors in various medical imaging applications has grown to be of paramount importance [5, 6]. Positron Emission Tomography (PET) is one of the most powerful setup with large number of inorganic or organic γ-ray detectors in an array for this purpose [7–9]. From a fundamental perspective, the progress in nuclear and particle physics experimental studies has been made achievable through research and development focused on the technical aspects of efficient and high-resolution γ-ray detector arrays [10–17]. The efficiency in detecting γ-ray and collecting charge carriers in HPGe detectors, particularly at lower gamma energies, tends to diminish over time. The primary cause for this decline is radiation damage, which may result from factors like neutron exposure during in-beam experiments or prolonged periods of cooling for older HPGe detectors. As a consequence, the thickness of the inactive dead layer increases as time passes [18–22]. For the case of the scintillator detector, the possible effects of radiation damage are i) radiation-induced absorption, ii) radiation-induced phosphore-scence, and iii) damage in scintillation mechanism. Among these, the color center formations and radiation-induced absorption are dominant for the radiation damage effect of the scintillator crystal [23]. To maintain a continuous assessment of the detectors in large detector facilities, it is imperative to monitor the responses of scintillator, segmented, or single-crystal HPGe γ-ray detectors over time. To obtain the variations in efficiency across the crystals, measurements of surface scans have been conducted using collimated low and high-energy γ-rays [24]. Indeed, these measurements require considerable time and precise alignments. Scanning a γ-ray detector by projecting interaction points onto a position-sensitive detector in coincidence provides a relatively expedient approach to assess performance across the crystal. Additionally, the pulse shape analysis (PSA) method serves as a valuable means to gauge the collection efficiency of charge carriers at specific positions within the crystal [25]. The electronic response, hole mobility, and features of the grid search algorithm have been investigated by L. Lewandowski, et al [26], and B. De Canditiisa et al [27].

In this work, we have scanned a single-crystal coaxial HPGe detector by a position-sensitive cerium-doped GAGG (Gadolinium Aluminum Gallium Garnet ($Gd_3Al_2Ga_3O_{12}$:Ce)) scintillator-based scanning setup with a ^{22}Na source. By analyzing and comparing the 2D scanned images from different sector (position) gates, we have examined the efficiency, actively seeking out defective regions along the γ-

ray interaction path within the crystal. The method has been demonstrated through GEANT4 simulation, showcasing its effectiveness in identifying defective regions within the detector. In practical terms, this approach offers a straightforward, rapid, and effective means to evaluate the performance and the current health status of a γ-ray detector of interest.

II. Instrumentation and Experimental Setup

A cerium-doped GAGG crystal has been coupled with a position-sensitive photomultiplier tube (Hamamatsu-8500C) to perform scans on a single-crystal coaxial reverse-electrode HPGe detector. The GAGG:Ce crystal offers several advantages, including minimal internal radioactivity, high light output (46,000–50,600 photons/1 MeV), a high density of 6.63 gm/cm^3, excellent radiation hardness, rapid timing characteristics, non-hygroscopic properties, and relative affordability. The crystal has dimensions of 5.08 × 5.08 × 0.6 cm^3. The position-sensitive photomultiplier tube consists of 64 readouts, organized in an 8 x 8 mesh of horizontal and vertical anode wires. These 64 readouts have been reduced to just 4 readouts by adding an appropriate external resistive chain network. The interaction positions of the γ-rays within the GAGG:Ce crystal were determined based on the four anode signals, which were previously discussed in our reports [28,29]. The single-crystal HPGe and GAGG:Ce detectors were biased at -3000 and -1100 V, respectively. For coincidence measurements, a ^{22}Na radioactive point source with an activity of approximately 270 kBq was employed. This source simultaneously emits two 511 keV γ-rays in opposite directions following the electron–positron annihilation of para-Positronium [30]. Both detectors were positioned on opposite sides of the source within the same horizontal plane and in the same coaxial line, maintaining suitable distances between them. The basic geometry of the setup is illustrated in Fig. 1.

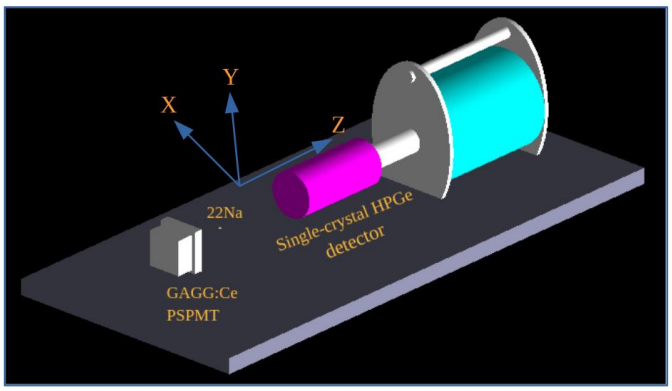

Fig. 1. Setup in GEANT4 geometry with a position-sensitive GAGG:Ce and a single-crystal HPGe detector. The ^{22}Na source is placed at 6 cm from GAGG:Ce and 12 cm from the single-crystal HPGe detector in the same line on a same horizontal plane.

The dynode and anode signals underwent amplification and shaping via spectroscopic amplifiers. A master gate was generated using the Constant Fraction Discriminator (CFD) outputs of the GAGG:Ce dynode and the single-crystal HPGe signal. The four anode signals (positions) were recorded when they fell within the specified time window of the master gate. The analog outputs from the spectroscopic amplifiers were digitized using an 8-channel, 12-bit Analog to Digital Converter (ADC) module. Experimental data were collected through the Linux Advanced Multi-Parameter System (LAMPS) [31] package. The complete dataset was analyzed using a C++-based macro within the ROOT-CERN software [32].

III. GEANT4 Simulation

The simulation performance was achieved using an object-oriented Monte Carlo simulation toolkit known as GEANT4, specifically version 4.10.05 [33]. Different parts of the setup were constructed using classes such as G4Box, G4Tubs, G4UnionSolid, G4SubtractionSolid, G4EllipticalTube, and G4Sphere within GEANT4. Fig. 1 provides a visualization of the setup's geometry in GEANT4. The ^{22}Na source, enclosed by a plastic disc, was defined within the simulation. In each event of a run, two simultaneous opposite 511 keV and a 1274 keV γ-rays were emitted in random directions from the source. Compton-scattered γ-rays, electrons, and positrons were expected to be generated during interactions of γ-rays with matter. In the PhysicsList, all potential physics processes for γ-rays, electrons, and positrons were considered. The primary interactions of γ-rays with matter included Compton scattering, the photoelectric effect, pair production, and Rayleigh scattering. Electrons and positrons produced during these interactions could undergo processes such as ionization, multiple scatterings, and emit Bremsstrahlung radiation. In addition, the positrons can annihilate with the surrounding electrons and emit two simultaneous 511 keV γ-rays. Within the PhysicsList, classes such as G4PhotoElectricEffect, G4Compton-Scattering, G4GammaConversion, and G4RayleighScattering were included for simulating γ-ray interactions. For electron and positron interactions with matter, the code considered classes such as G4eMultipleScattering, G4eIonisation, G4eBremsstrahlung, and G4eplusAnnihilation. The simulation results were stored in a ROOT NTuple on an event-by-event basis and were analyzed using a ROOT macro.

IV. Analysis and Result

The energy calibrations of the γ-ray spectra from both detectors were performed using a ^{152}Eu radioactive source with well-known gamma energies ranging from 100 to 1500 keV. Notably, there was no significant internal radioactivity detected in the GAGG:Ce scintillator. The (X, Y) interaction points on the GAGG:Ce crystal were calculated based on the four anode signals using two equations [28]. A Full Width at Half Maximum (FWHM) of approximately 3 mm was determined with a 2 mm collimated ^{22}Na source positioned at the center of the crystal. The FWHM exhibited a slight deterioration as one moved away from the center towards the edge. The energy resolutions at 511 keV for GAGG:Ce and HPGe were determined to be approximately 15% and 0.2%,

respectively. The 2D scanned images of the front-face and side-face were reconstructed with the energy gates set of 505 keV < $E_{\gamma:HPGe\ \&\ GAGG}$ < 516 keV. Both experimental (with a full bias of -3000 V) and simulated 2D images of the front scan are presented in Fig. 2. Notably, the reduced efficiency in the middle of the images highlights the presence of an axial cavity.

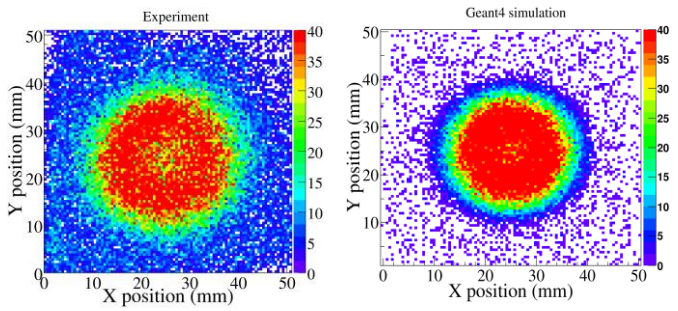

Fig. 2. Measured (left) and simulated (right) scanned images of the front face reconstructed with an energy gate of 511 keV ($E_{\gamma:HPGe\ \&\ GAGG}$: 506-516 keV) on both the detectors. In the measured image, some background counts are there throughout the GAGG:Ce crystals because of the lower amplitude anode noise and random coincidences.

The incidence direction of the γ-ray in the HPGe crystal is well defined by a position gate on a sector (white mark on white rectangle on inset of Fig. 3) of the scanned image. Along that defined path, the 511 keV γ-ray interacts with the HPGe crystal via the photoelectric effect or Compton scattering. Irrespective of the nature of the interaction, the first interaction points will lie along this defined path. Depending upon the energy deposition condition in the HPGe detector, the effective depth of the trajectory will be different. This is simulated in GEANT4 and has been shown in Fig. 3. The image actually shows a 2D projection of the trajectory of the γ-rays having the first interaction within the HPGe crystal which are in coincidence with the GAGG:Ce detector. The interaction positions have been filled in the 2D histogram (Y-Z plane of single HPGe detector) in each step of interaction based on energy deposition in the crystal.

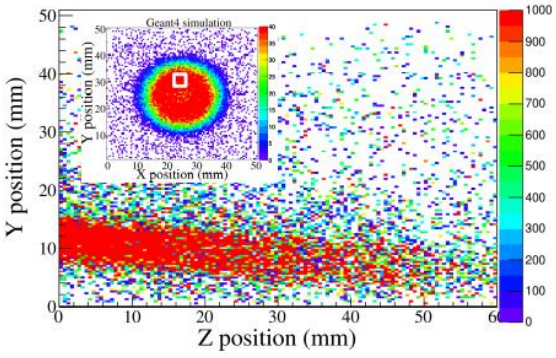

Fig. 3. The simulated interaction positions (in X-Z plane) of the γ-rays inside the single HPGe crystal obtained with a small position sector gate (shown in a white square of the inset 2D image) in the image formed by the GAGG detector.

A demonstration of the scanning results in the presence of a defective region within the crystals was illustrated through GEANT4 simulation. In this simulation, a dead region measuring 1 cm^3 was introduced into the HPGe crystal, as depicted in Fig. 4(a). The simulation was conducted for various locations (P1 to P6, marked as black dots) within the dead region.

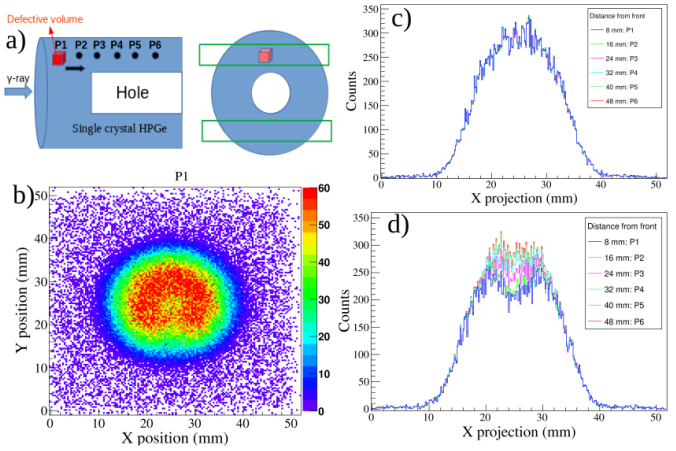

Fig. 4. a) The schematic of the single-crystal HPGe. A small (1 cm^3) dead region (in red) has been introduced on the upper side. The simulation has been run for different position of the dead region from P1 to P6, b) The 2D scanned image when the dead region is placed at P1. The projections of the slices of 2D image on c) upper portion where all histograms superposed, d) lower portion which has been shown up with lower efficiency due to presence of dead region.

In this scenario, a 2D scanned image of the front face (refer to Fig. 4(b)) was reconstructed by the GAGG:Ce detector in coincidence with the HPGe detector. The X-projections of a slice on the upper side of this 2D image, considering different locations of the defective region, are displayed in Fig. 4(c). It's noteworthy that all the projected histograms overlap, signifying the absence of a dead region on the lower portion of the HPGe crystal. However, the projected histograms of the bottom slices (Fig. 4(d)) reveal deviations in efficiency, indicating the presence of a dead region within the upper volume of the HPGe crystal. The method allows for the identification of such deviations by adjusting gates on all sides. These histograms also highlight that the described method possesses a sensitivity limit for detecting the existence of a defective region, approximately 1 cm^3 in volume, within the crystal. This limitation arises due to the absorption profile of 511 keV γ-rays within the crystal. Based on the present GEANT4 results, the sensitivity limit extends up to a depth of 40 mm from the crystal's entry surface. This limit can be adjusted depending on the density and material of the crystal. For larger crystals, scanning different surfaces may be required to surpass this limit. Notably, from the experimental 2D image, no defective regions were identified within the used single-crystal HPGe detector.

V. Conclusions

A single-crystal coaxial HPGe detector has been scanned by a position-sensitive GAGG:Ce detector. The 2D scanned images have been obtained with an energy gate of 511 keV. The simulated scanned images are consistent with the experimentally measured images. Due to some low amplitude noise of the anode signals and random coincidence, the experimental image has random background throughout the crystal. The incident direction of the γ-ray in the HPGe crystal is well defined by a position gate on a sector on the GAGG:Ce detector. Irrespective of the nature of the interaction, the first interaction points will lie along a defined path. In the GEANT4 simulation, a defective region has been introduced within the HPGe crystal. Coincidence images have been generated for varying locations of this defective region. The defective region is clearly discernible in the corresponding image as it exhibits reduced efficiency, which is further reflected in the projection of the simulated 2D spectrum. Analysis of the experimentally obtained images reveals uniform efficiency around the center, indicating the absence of any defective regions within the employed single-crystal HPGe. However, the simulation results suggest that this method has a sensitivity limitation for identifying defective regions, typically in the vicinity of 1 cm^3 in volume, within the Ge crystal. This limitation is primarily restricted to a depth of 40 mm from the surface but may vary when applied to different crystal types, making it a subject of ongoing interest.

Acknowledgment

Authors would like to thank the funding agency, Department of Atomic Energy (DAE), Government of India (Project Identification No. RTI 4002) and Department of Science and Technology (DST), Government of India (project No. IR/S2/PF-03/2003-II), respectively. B.D would also like to thank Infosys-TIFR Leading Edge Travel Grant.

References

[1] R. W. Todd, J. M. Nightingale, and D. B. Everett, "A proposed γ camera", Nature **251**, 132–134, (1974).
[2] S. Jan, G. Santin, D. Strul, S. Staelens, K. Assié, et al., "GATE: a simulation toolkit for PET and SPECT," Phys. Med. Biol., vol. **49**, no. 19, pp. 4543–4561, (2004).
[3] S. R. Cherry, T. Jones, J. S. Karp, J. Qi, W. W. Moses, and R. D. Badawi, "Total-Body PET: Maximizing Sensitivity to Create New Opportunities for Clinical Research and Patient Care", J. Nucl. Med., vol. **59**, no. 1, pp. 3–12, 2018.
[4] P. Moskal, K. Dulski, N. Chug, et al., "Positronium imaging with the novel multiphoton PET scanner", Sci. Adv. 2021; **7**: eabh4394.
[5] T. Tanimori, Y. Mizumura, A. Takada, *et al.,* "Establishment of Imaging Spectroscopy of Nuclear Gamma-Rays based on Geometrical Optics", Sci. Rep. **7** 41511 (2017).
[6] E. K. Leung, M. S. Judenhofer, S. R. Cherry, and R. D. Badawi, "Performance assessment of a software-based coincidence processor for the EXPLORER total-body PET scanner", Phys. Med. Biol., vol. **63**, no. 18, p. 18NT01, 2018.
[7] Terry Jones and David Townsend, "History and future technical innovation in positron emission tomography", Journal of Medical Imaging, vol. **4**, no. 1, p. 011 013, Mar. 2017.
[8] N. A. Mullani, J. Gaeta, K. Yerian, W. H. Wong, R. K. Hartz, et al., "Dynamic Imaging with High Resolution Time-of-Flight PET Camera-TOFPET I", IEEE Transactions on Nuclear Science **31**, 1, 609-613 (1984).
[9] P. Moskal, D. Kisielewska, C. Curceanu, E. Czerwiński, K. Dulski, A. Gajos, et al., "Feasibility study of the positronium imaging with the J-PET tomograph", Phys. Med. Biol., vol. **64** no. 5, 055017 (2019).
[10] G. S. Li, C. Lizarazo, J. Gerl, I. Kojouharov, H. Schaffner, M. Górska, N. Pietralla, S. Saha, M. L. Liu, and J. G. Wang, "Simulated characteristics of the DEGAS γ-detector array", Nucl. Instrum. Methods A **890** (2018) 148-154.
[11] M. Rudigier, Zs. Podolyák, P. H. Regan, A. M. Bruce, S. Lalkovski, R. L. Canavan, E. R. Gamba, O. Roberts, I. Burrows, D. M. Cullen, L. M. Fraile, L. Gerhard, J. Gerl, M. Gorska, A. Grant, J. Jolie, V. Karayonchev, N. Kurz, W. Korten, I.H. Lazarus, C. R. Nita, V. F. E. Pucknell, J.-M. Régis, H. Schaffner, J. Simpson, P. Singh, C. M. Townsley, J. F. Smith, and J. Vesic, "FATIMA — FAst TIMing Array for DESPEC at FAIR", Nucl. Instrum. Methods A **969** (2020) 163967.
[12] S. Akkoyun, et al., "AGATA—Advanced GAmma Tracking Array", Nucl. Instrum. Meth. A **668**, 26 (2012).
[13] J. Simpson, "The Euroball Spectrometer", Z. Phys. A **358**, 139 (1997).
[14] I. Y. Lee, "The GAMMASPHERE", Nucl. Phys. A **520**, 641 (1990).
[15] R. Palit, "Recent results from digital INGA at BARC–TIFR Pelletron Linac Facility and future plans", Pramana **83**, 719-728 (2014).
[16] I. Y. Lee and J. Simpson, "AGATA and GRETA: The Future of Gamma-Ray Spectroscopy", Nucl. Phys. News Intl. **20**, 23-28 (2010).
[17] J. Eberth, et al., "MINIBALL: A Ge detector array for radioactive ion beam facilities", Prog. Part. Nucl. Phys. **46**, 389 (2001).
[18] J. Ródenas, A. Pascual, I. Zarza, V. Serradell, Josefina Ortiz, and L. Ballesteros, "Analysis of the influence of germanium dead layer on detector calibration simulation for environmental radioactive samples using the Monte Carlo method", Nucl. Instrum. Methods A **496** (2003) 390–399.
[19] A. Elanique, O. Marzocchi, D. Leone, L. Hegenbart, B. Breustedt, and L. Oufni, "Dead layer thickness characterization of an HPGe detector by measurements and Monte Carlo simulations", Appl. Radiat. Isot. **70** (2012) 538–542.
[20] E. Andreotti, M. Hult, G. Marissens, G. Lutter, A. Garfagnini, S. Hemmer, K. von Sturm, "Determination of dead-layer variation in HPGe detectors", Appl. Radiat. Isot. **87** (2014) 331–335.
[21] Truong Thi Hong Loan, Vu Ngoc Ba, Truong Huu Ngan Thy, Huynh Thi Yen Hong, Ngo Quang Huy, "Determination of the dead-layer thickness for both p- and n-type HPGe detectors using the two-line method", Journal of. Radioanal. Nucl. Chem. **315** (2018) 95–101.
[22] Mikael Hult, Stef Geelen, Mark Stals, Guillaume Lutter, Gerd Marissens, Heiko Stroh, Sonja Schreurs, Wouter Schroeyers, Michel Bruggeman, Leen Verheyen, "Determination of homogeneity of the top surface deadlayer in an old HPGe detector", Appl. Radiat. Isot. **147** (2019) 182–188.
[23] Ren-yuan Zhu, "Radiation damage in scintillating crystals", Nucl. Instrum. Methods A **413** (1998) 327-311.
[24] B. De Canditiis,G. Duchene, M. H. Sigward, M. Filliger, F. Didierjean, M. Ginsz, D. Ralet, "Full-volume characterization of an AGATA segmented HPGe gamma-ray detector using a ^{152}Eu source", Eur. Phys. J. A **57** (2021) 223.
[25] F. C. L. Crespi, F. Camera, B. Million, M. Sassi, O. Wieland, A. Bracco, "A novel technique for the characterization of a HPGe

detector response based on pulse shape comparison", Nucl. Instrum. Methods A **593** (2008) 440– 447.

[26] L. Lewandowski, P. Reiter, B. Birkenbach, B. Bruyneel, E. Clement, J. Eberth, H. Hess, C. Michelagnoli, R.M. Perez-Vidal, and M. Zielinska, "Pulse-Shape Analysis and position resolution in highly segmented HPGe AGATA detectors", Eur. Phys. J. A (2019) **55**: 81.

[27] B. De Canditiisa, G. Duchêne, "Simulations using the pulse shape comparison scanning technique on an AGATA segmented HPGe gamma-ray detector", Eur. Phys. J. A **56** (2020) 276.

[28] Biswajit Das, R. Palit, R. Donthi, A. Kundu, Md. S. R. Laskar, P. Dey, D. Negi, F. S. Babra, S. Jadhav, B. S. Naidu, and A. T. Vazhappilly, "Development of a position-sensitive fast scintillator ($LaBr_3$(Ce)) detector setup for gamma-ray imaging application", EPJ Web Conf. **253** (2021) 11005.

[29] Biswajit Das, A. Kundu, R. Palit, V. Malik, P. Dey, D. Negi, S.K. Jadhav, A. T. Vazhappilly, and B. S. Naidu, "Development of a GAGG(Ce)-based compact 3D scanning setup for assessment of active volume in γ-ray detectors", Nucl. Instrum. Meth. A **1048** (2023) 167928.

[30] NNDC, 2022, http://www.nndc.bnl.gov/nudat2.

[31] TIFR homepage URL http://www.tifr.res.in/~pell/lamps.html.

[32] Root-CERN homepage URL https://root.cern/.

[33] Geant4-CERN homepage URL https://geant4.web.cern.ch/.